40. K. Rages and J. B. Pollack, *Icarus* **41**, 119 (1980).
41. M. Tomasko, *J. Geophys. Res.* **85**, 5937 (1980).
42. A. L. Lane *et al.*, *Science* **215**, 537 (1982).
43. D. Strobel, *Planet. Space Sci.*, in press.
44. W. R. Ward, *Icarus* **46**, 97 (1981).
45. J. A. Van Allen, M. F. Thomsen, B. A. Randall, R. L. Rairden, C. L. Grosskreutz, *Science* **207**, 415 (1980); J. A. Simpson *et al.*, *J. Geophys. Res.* **85**, 5731 (1980).
46. *Int. Astron. Union Circ. 3457* (6 March 1980).
47. *Ibid., No. 3466* (10 April 1980).
48. *Ibid., No. 3496* (31 July 1980).
49. E. C. Stone, *Nature (London)* **292**, 675 (1981).
50. ——— and E. D. Miner, *Science* **215**, 499 (1982).
51. G. L. Tyler *et al.*, *ibid.*, p. 553.
52. Y. Kozai, *Publ. Astron. Soc. Jpn.* **28**, 675 (1976).
53. D. P. Cruikshank, *Rev. Geophys. Space Phys.* **79**, 165 (1979); R. N. Clark and P. D. Obensby, in preparation; U. Fink *et al.*, *Astrophys. J. Lett.* **207**, 63 (1976).
54. G. E. Danielson *et al.*, *J. Geophys. Res.* **86**, 8683 (1981).
55. A. Dollfus, *Astronomie* **6**, 2534 (1968); J. W. Fountain and S. M. Larson, *Icarus* **36**, 92 (1978).
56. C. F. Yoder, *Nature (London)* **279**, 767 (1979).
57. S. J. Peale, P. Cassen, R. T. Reynolds, *Science* **203**, 892 (1979).
58. C. Yoder, *Eos*, in press.
59. A. F. Cook and R. J. Terrile, in preparation.
60. D. L. Stevenson and A. Anderson, *Eos*, in press.
61. D. P. Cruikshank and R. H. Brown, *Icarus*, in press.
62. S. Soter, paper presented at the IAU Planetary Satellite Conference, Cornell University, Ithaca, N.Y., 1974.
63. D. P. Cruikshank, in preparation.
64. A. F. Cook and F. A. Franklin, *Icarus* **13**, 282 (1970).
65. J. Degewij, J. Gradie, B. Zellner, *Bull. Am. Astron. Soc.* **9**, 503 (1977).
66. E. M. Shoemaker, in *The New Solar System*, J. K. Beatty, B. O'Leary, A. Chaikin, Eds. (Sky, Cambridge, Mass., and Cambridge Univ. Press, 1981), pp. 117–128; E. M. Shoemaker and R. F. Wolfe, *Lunar Planet. Sci.* **12** (Suppl. A), 1 (1981).
67. E. M. Shoemaker and R. F. Wolfe, in *The Satellites of Jupiter*, D. Morrison, Ed. (Univ. of Arizona Press, Tucson, in press).
68. J. H. Oort, *Bull. Astron. Inst. Neth.* **2**, 91 (1950); P. R. Weissman, in *Comets, Asteroids, Meteorites*, A. H. Delsemme, Ed. (Univ. of Toledo Press, Toledo, Ohio, 1977), pp. 87–91.
69. J. S. Lewis, *Science* **172**, 1127 (1971); *Sci. Am.* **230** (No. 3), 50 (1974); *Space Sci. Rev.* **14**, 401 (1973).
70. M. J. Lupo and J. S. Lewis, *Icarus* **40**, 157 (1979).
71. A. S. Grossman, J. B. Pollack, R. T. Reynolds, A. L. Summers, H. C. Graboske, Jr., *ibid.* **42**, 358 (1980).
72. J. B. Pollack, A. S. Grossman, R. Moore, H. C. Graboske, Jr., *ibid.* **29**, 35 (1976).
73. P. Bodenheimer, A. S. Grossman, W. DeCampli, G. Marcy, J. B. Pollack, *ibid.* **41**, 293 (1980).
74. A. G. W. Cameron and J. B. Pollack, in *Jupiter*, T. Gehrels, Ed. (Univ. of Arizona Press, Tucson, 1976), p. 61.
75. J. S. Lewis, *Icarus* **16**, 241 (1972).
76. R. Prinn and B. Fegley, *Astrophys. J.*, in press.
77. J. N. Cuzzi and J. B. Pollack, *Icarus* **33**, 233 (1977).
78. J. Lissauer, F. H. Shu, J. N. Cuzzi, *Nature (London)* **292**, 707 (1981); M. Hénon, *ibid.* **293**, 33 (1981).
79. J. B. Pollack, J. A. Burns, M. E. Tauber, *Icarus* **37**, 587 (1979).
80. W. Slattery, *ibid.* **32**, 58 (1977).
81. S. A. Collins *et al.*, *Nature (London)* **288**, 439 (1980).
82. J. E. Keeler, *Astron. J.* **8**, 175 (1889).
83. W. A. Baum *et al.*, *Icarus* **47**, 84 (1981).
84. J. N. Cuzzi *et al.*, *Nature (London)* **292**, 703 (1981).
85. F. A. Franklin and A. F. Cook, in preparation.
86. J. Lukkari, *Nature (London)* **292**, 433 (1981); D. N. C. Lin and P. Bodenheimer, *Astrophys. J. Lett.* **248**, L83 (1981); W. R. Ward, *Geophys. Res. Lett.* **8**, 641 (1981).
87. P. Goldreich, private communication.
88. ——— and N. Borderies, private communication; M. Showalter, *Bull. Am. Astron. Soc.* **13**, 728 (1981).
89. R. J. Terrile *et al.*, *Bull. Am. Astron. Soc.* **13**, 728 (1981).
90. With the completion of the second Voyager Saturn encounter, the Voyager spacecraft have now returned more than 62,000 images of Jupiter, Saturn, and their entourages. More than a random accumulation of photographs, these images constitute carefully planned and executed time-lapse sequences of atmospheric, volcanic, or ring activity, multispectral mosaics of geologic surfaces, or extensive scans of small-scale ring structure. This treasure of stunning and informative pictures greatly exceeds the original imaging plans for Voyager and represents the successful efforts of several thousand talented individuals who have devoted their skills to this mission. A few of these people, those who are directly associated with this report, are listed below. J. B. Plescia (crater counts); L. A. Sromovsky (Saturn and Titan measurements); P. Thomas (satellite radiometry); T. C. Duxbury (Hyperion); P. Goldreich, J. J. Lissauer, E. Grün, G. Morfill (ring structure and formation); S. W. Squyres (geology); J. L. Anderson, P. L. Jepsen, and G. M. Yagi (image processing); G. W. Garneau (atmospheric feature tracking for sequence predictions); G. P. Dimit, L. Garcia, D. Godfrey, A. Piumpunyalerd, E. T. Simien, and E. S. Thompson (data handling and manuscript preparation); JPL's photolab and graphics departments, Image Processing Laboratory, and Mission and Test Imaging System; and two reviewers, including M. J. S. Belton. G.E.H. is supported by the Science and Engineering Research Council, Great Britain. This report presents the results of one phase of research carried out at the Jet Propulsion Laboratory under NASA contract 7-100.

30 November 1981

Photopolarimetry from Voyager 2: Preliminary Results on Saturn, Titan, and the Rings

Abstract. *The Voyager 2 photopolarimeter was reprogrammed prior to the August 1981 Saturn encounter to perform orthogonal-polarization, two-color measurements on Saturn, Titan, and the rings. Saturn's atmosphere has ultraviolet limb brightening in the mid-latitudes and pronounced polar darkening north of 65°N. Titan's opaque atmosphere shows strong positive polarization at all phase angles (2.7° to 154°), and no single-size spherical particle model appears to fit the data. A single radial stellar occultation of the darkened, shadowed rings indicated a ring thickness of less than 200 meters at several locations and clear evidence for density waves caused by satellite resonances. Multiple, very narrow strands of material were found in the Encke division and within the brightest single strand of the F ring.*

Shortly after it left the Jupiter system and successfully acquired ultraviolet data on the Great Red Spot and the Jovian clouds (*1*, *2*), the Voyager 2 photopolarimeter (PPS) experienced several operational difficulties. These were associated with the command-decoding processes, which control the analyzer and filter wheel positions (*3*). Extensive testing during the Jupiter-to-Saturn cruise phase of the Voyager 2 trajectory demonstrated several viable methods of instrument operation to accommodate these new PPS command modes. The data-acquisition technique used at Saturn generated measurements that had the following characteristics: (i) two-color character, ultraviolet at 2640 ± 150 Å and deep red at 7500 ± 125 Å; (ii) orthogonal linear polarizations for each color sampled; and (iii) an eightfold increase in count rate discriminability for stellar occultation measurements. These enhanced performance characteristics made it possible for the Voyager 2 PPS to successfully measure the scattering properties of the Saturn and Titan atmospheres, as well as to make a single radial stellar occultation of Saturn's rings, and to measure partial phase curves for Iapetus, Rhea, Enceladus, and Phoebe.

The unfortunate scan platform anomaly that occurred near the crossing of the ring plane prevented acquisition of high-phase-angle data on Saturn and on all the satellites except Titan (*4*). Those partially completed studies will require more sophisticated analyses (*5*). This report contains the initial results from the Saturn and Titan atmospheric scattering studies and the δ Scorpii stellar ring occultation.

Saturn's atmosphere. During the approach phase of the Voyager 2 spacecraft to Saturn, the PPS measured the intensity and polarization of light from Saturn. The instrument used an ultraviolet wavelength filter, 2640 Å, with a bandpass of 300 Å, and an infrared wavelength filter, 7500 Å, with a bandpass of 250 Å. In this report we discuss intensity measurements obtained for a portion of the east-west map of the northern hemisphere and a north-south measurement swath that gives information about the general reflectivity characteristics of Saturn's central meridian. Data for the east-west map were obtained during the Saturn approach at a distance of 4.2×10^6 km and a phase angle of 10.1°. The PPS instrument footprint is circular and had a diameter of 8000 km at this distance for the instrument's 0.11° field of view. The north-south data were obtained at a distance of 1.6×10^6 km and a phase angle of 17.0°, with the instrument footprint equal to 3100 km.

Figure 1a shows the 7500-Å east-west map of Saturn. The intensity is color-coded, with the highest count levels represented by white and the lower count levels represented by dark red. The brightest region on Saturn occurs near the equator just left of center, at the

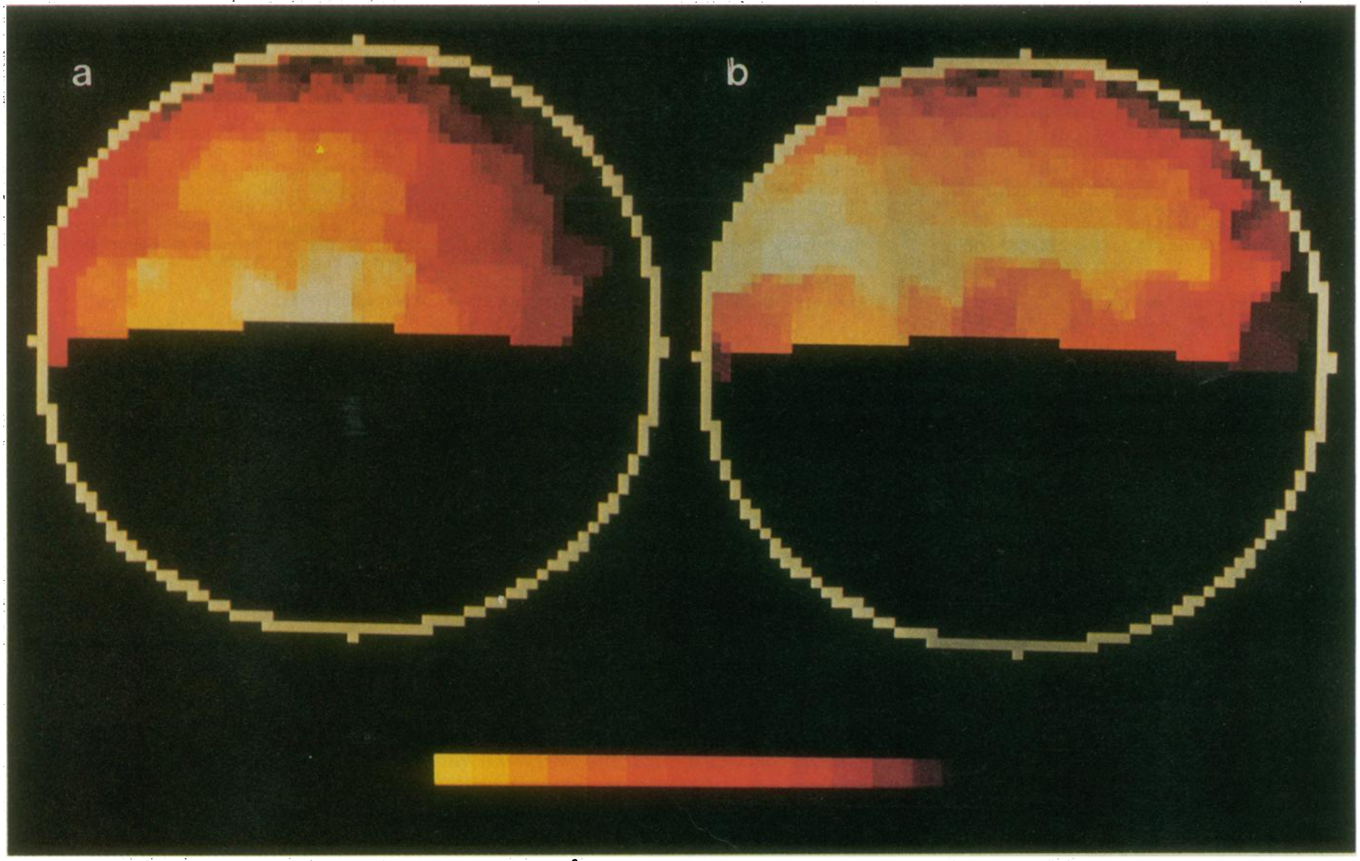

Fig. 1. (a) Map of the northern hemisphere of Saturn at 7500 Å. The brightness is color-coded, with the brightest areas white and the darkest areas dark red. (b) Saturn northern hemisphere map at 2640 Å. In the color table at the bottom the highest values are on the left.

subsolar point. The essential center-to-limb variation is close to that of a Lambert surface, similar to the behavior seen at visible red wavelengths. The 2640-Å intensity map in Fig. 1b shows limb brightening, with the highest intensity occurring at the left, west limb (bright limb). Qualitatively, the limb darkening behavior at 7500 and 2640 Å is similar to imaging data obtained by Voyager 1 and Voyager 2 through orange (6140 Å) and ultraviolet (3500 Å) filters (*6*).

At 7500 Å, photons are scattered by the cloud particles of the Saturn atmosphere. At this wavelength contrasts are produced by variations in cloud properties. At 2640 Å, both variations in cloud scattering properties and aerosol vertical distributions contribute to the observed contrast and center-to-limb characteristics. The limb brightening seen at mid-latitudes is similar to the behavior of Jupiter's Equatorial Zone and North Tropical Zone as observed by the same instrument at 2400 Å. By analogy with our understanding of Jupiter's atmosphere (*1, 2*), the absorbers in Saturn's mid-latitudes are distributed through a wide range of altitudes and are probably concentrated below the 100-mbar level. Saturn's ultraviolet reflectivity differs from Jupiter's in one very important respect. Jupiter's central meridian reflectivity drops much faster than Saturn's poleward of 30° latitude.

The higher resolution north-south swath, although insufficient to permit construction of a two-dimensional map, provides a better characterization of the high-latitude ultraviolet absorption on Saturn. Figure 2 shows the instrument counts (proportional to intensity) for the north-south measurements as a function of latitude along the subspacecraft meridian. The contrast reversal of the prominent belt at 21°N, noted by the Voyager 1 imaging investigators (*6*), is even more prominently seen at the PPS wavelengths. The data gap from the equator to 30°S occurs where the rings of Saturn prevent viewing of the atmosphere.

The latitudinal ultraviolet brightness shows a sharp change in character at about 65°N. Figure 3 shows two models that demonstrate how the 2640-Å data constrain the altitude occurrence of absorption in Saturn's atmosphere. The homogeneously mixed model has absorbers mixed uniformly (by number) with gas in the Saturn atmosphere. The vertical axis in Fig. 3, for homogeneous models, indicates the pressure level where a total optical depth of unity is reached at each latitude. A homogeneously mixed model with a latitudinally independent mixing ratio fits the east-west map data to 65°N reasonably well. However, the north-south map data show that the mixing ratio of absorbers increases northward of 65°N, raising the level where the total optical depth is equal to unity at 80 mbar near the north pole. Alternatively, the atmosphere can be completely absorbing to a pressure level of about 20 mbar with clear molecular gas above this pressure level (the pure Rayleigh scattering model in Fig. 3). Either one of these points of view indicates the presence of strong high-altitude, polar-region absorption in Saturn's atmosphere.

We believe that a consistent physical picture of Saturn ultraviolet absorption is obtained if one assumes that the accumulation of high-altitude absorbers in the polar region of Saturn is the consequence of auroral bombardment leading to the formation of hydrocarbon molecules. This is the same physical picture that we believe applies to Jupiter's polar ultraviolet absorption (*7*). Morphological differences in auroral energetic particle bombardment on Saturn and Jupiter are manifested in the distribution of complex hydrocarbon molecular absorbers that can be in the form of small particulates. In this picture, the auroral zones on Saturn and Jupiter map directly into ultraviolet absorption as a result of the formation of hydrocarbons having double and triple carbon-carbon bonds. In the case of Saturn, the dark ultraviolet imprint of the auroral zone is confined to latitudes north of 65°N. This is consistent with the confined Saturn auroral zone shown by Voyager observations in atomic hydrogen Lyman α radiation (*8*). The ultraviolet dark imprint of the auroral zone on Jupiter extends to mid-latitudes, consistent with the lower latitude occurrence of Jovian aurora associated with the Io flux tube and the Jovian magnetotail and their wanderings in latitude with the offset magnetic field (*9*). It is certain that some of the energetic particle energy input may be available for the destruction of methane or the onset process leading to the formation of hydrocarbons or organic molecules in the Saturn and Jupiter atmospheres. The precise amount depends upon the turbopause level in the polar regions of Saturn and Jupiter. With the long transport time constants on these planets, the accumulation of ultraviolet-absorbing material may occur.

Titan. We made photometry and polarization measurements of Titan by using filters with effective wavelengths of 2640 and 7500 Å. Integrated disk measurements were obtained with a 1° diameter field of view at many phase angles between 2.7° and 154°. One set of spatially resolved measurements was obtained with a 0.11° diameter field of view when Titan's diameter and phase angle were, respectively, 0.42° and 85° (*10*).

Most Titan observations were about 20 minutes in duration. During the observing period, the filter wheel and polarization analyzer wheel were stepped on 24-second centers. At phase angles higher than 25°, uncertainty in the data from statistical fluctuations is quite small because of the large number of 0.4-second integrations and the high counting rate (up to 1800 counts per integration at 2640 Å and 30,000 counts per integration at 7500 Å). For those data, the largest source of error arises from instrumental effects such as electronic hysteresis. We have noted the quantitative effect of instrumental biases on the polarization results in terms of the size of the error bars in Figs. 4 and 5. These may diminish with subsequent postencounter calibrations.

The two linear analyzers that were used have orthogonal orientation, permitting an unambiguous determination of

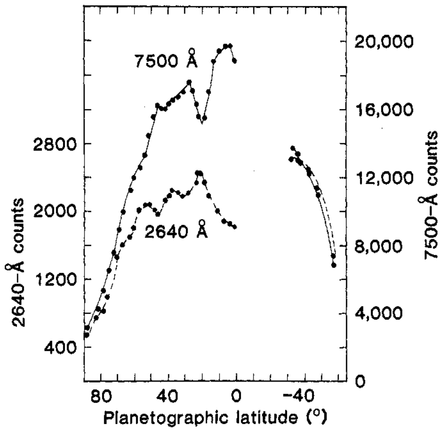

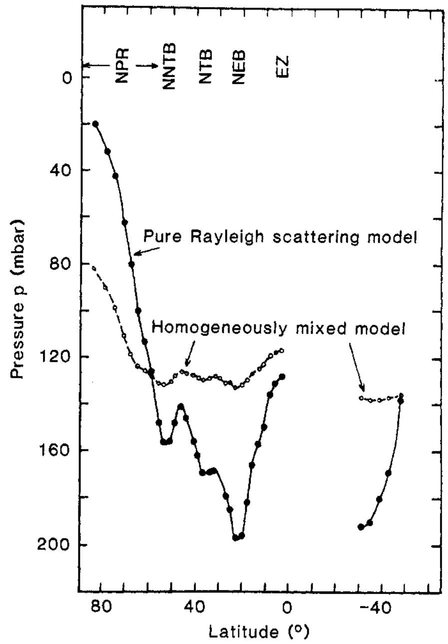

Fig. 2 (left). Photopolarimeter counts (proportional to brightness) for a north-south swath of data along the Saturn subspacecraft meridian. Fig. 3 (right). Two models applied to the north-south 2640-Å data; *NPR*, North Polar Region; *NNTB*, North North-Temperate Belt; *NTB*, North Temperate Belt; *NEB*, North Equatorial Belt; *EZ*, Equatorial Zone. The pure Rayleigh scattering model has nonabsorbing gas above a perfect absorber at pressure *p*. The homogeneously mixed absorbing model gives the pressure level where an optical depth of unity occurs in the Saturn atmosphere.

intensity ($I_1 + I_2$) (*11*). If the linear polarization is either parallel or perpendicular to the scattering plane, the magnitude and sign of the linear polarization can be derived:

$$P = \frac{\sec(2\chi)(I_1 - I_2)}{I_1 + I_2}$$

where I_1 is the count rate in the analyzer most closely aligned with the normal to the scattering plane, and χ is the angle between the scattering plane and the analyzer orientation. The polarization is not determined when χ is 45° and is difficult to determine when χ is near 45°. The values of χ range from 1° at the 2.7° phase angle measurement to 39° at phase angle measurements from 66° to 117°, decreasing to 31° at a phase angle of 154°.

Observed polarizations at the two wavelengths are large and positive at all phase angles between 30° and 154° (Figs. 4 and 5). Polarization reaches a maximum near a phase angle of 90° and decreases monotonically at smaller and larger phase angles. This behavior was first observed by Pioneer 11 (*12*) at effective wavelengths of 4400 and 6400 Å and phase angles up to 95°. The polarization is highest at 2640 Å and decreases monotonically with wavelength to 7500 Å.

At 2640 Å, polarization from single-scattered light must be 85 percent to produce the observed polarization from

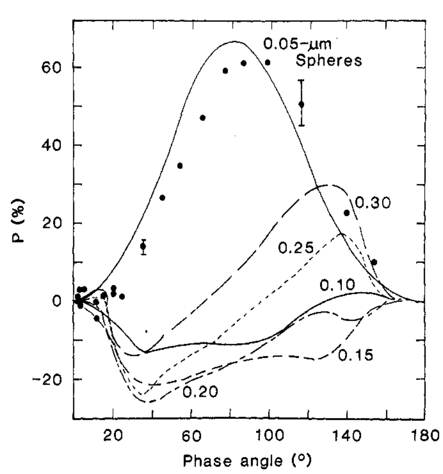

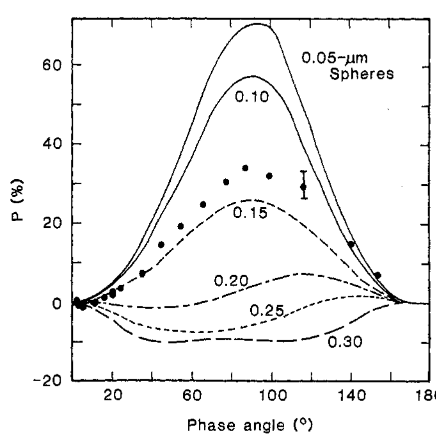

Fig. 4 (left). Integrated disk percent polarization for Titan at 2640 Å. Dots represent observations, and lines show calculations for homogeneous semi-infinite atmospheres with different sized spheres. Fig. 5 (right). Integrated disk percent polarization for Titan at 7500 Å. The models from Fig. 4 are also plotted.

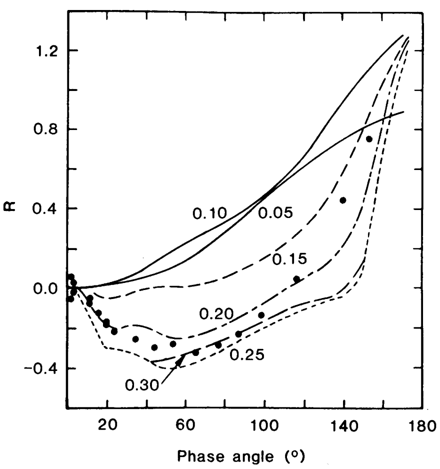

Fig. 6. Integrated disk color ratio (R) as a function of phase angle. The color ratio is expressed in the form

$$R = \log\left[\frac{F(2640\ \text{Å},\alpha)}{F(7500\ \text{Å},\alpha)}\right] - \log\left[\frac{F(2640\ \text{Å},0)}{F(7500\ \text{Å},0)}\right]$$

where πF is the observed count rate at phase angle α. The models from Figs. 4 and 5 are also shown.

multiply scattered light. The fraction of observed 2640-Å photons that interact with the molecular atmosphere above the cloud top is small, because the pressure level of the optical limb (*6*) is 0.3 mbar, giving an N_2 optical depth of only 0.005.

The importance of aerosol scattering on Titan has been emphasized by ground-based observers (*13–15*) and spacecraft observations (*6, 12*). The high polarization in Pioneer 11 4400-Å data led Tomasko to argue for a mean particle radius ($\bar{r}$) of about 0.08 μm (*12*). The dependence of Titan's geometric albedo between a phase angle of 0° and 6.4° at several wavelengths, and the observed brightness ratio of about 5 at 4200 Å from Voyager 1 phase angle measurements at 160° and 129°, indicate a value of $\bar{r}$ in the range 0.25 to 0.3 μm (*6, 15*).

In Figs. 4 and 5 we show polarization characteristics for model atmospheres having 0.05 μm $\leq \bar{r} \leq$ 0.3 μm. The real part of the refractive index, N_r = 1.7, was chosen to facilitate comparison with the models of Rages and Pollack (*15*). The imaginary part is determined from Titan's geometric albedo. We use the values 0.028 and 0.23 at 2640 and 7500 Å, respectively (*15, 16*). The final parameter for Mie scattering calculations is the size distribution parameter, b = 0.05 (*17*). The single-scattering phase matrix for each particle was used in a polarization doubling code (*18*) to compute scattering from a homogeneous semi-infinite cloud deck. Net polarization from the integrated disk was computed from Horak's (*19*) cubature formulas.

At 2640 Å, only particles as small as 0.05 μm in radius have the peak polarization values observed, although the shape of the 0.05-μm model is skewed to smaller phase angles with respect to the observations. Larger particles give polarizations much smaller than the observations at most phase angles.

The best fit to polarization data at 7500 Å is for spheres with $\bar{r} \cong$ 0.13 μm. Since these particles do not fit the 2640-Å data, we are forced to abandon the single-size spherical particle homogeneous model. A reasonable modification to the model is the concept of an altitude gradient in particle size (*20*).

A simple two-layer model with an optical depth τ of 0.05-μm spheres on top of a semi-infinite layer of 0.15-μm spheres gives the correct wavelength dependence of polarization because τ is proportional to the extinction efficiency of 0.05-μm spheres. The extinction efficiency varies by a factor of 70 from 2640 to 7500 Å. However, these model polarization curves are also skewed to smaller phase angles relative to the data.

An independent piece of information that can be used to measure particle size is the scattered flux πF as a function of phase angle and wavelength. Large particles have strongly forward-scattering phase functions and can have a backscattering peak as well. We have computed the 2640 Å/7500 Å color ratio of Titan and model atmospheres at a variety of phase angles (Fig. 6). The data are most consistent with spheres having 0.2 μm $\leq \bar{r} \leq$ 0.3 μm.

In our present state of analysis, we are facing the same difficulty that became apparent after the recent Pioneer 11 and Voyager 1 Titan encounters. The polarization and photometry data appear to give mutually exclusive results, although both data sets indicate particles with 0.05 μm $\leq \bar{r} \leq$ 0.3 μm if N_r = 1.7. If a single type of particle is responsible for the

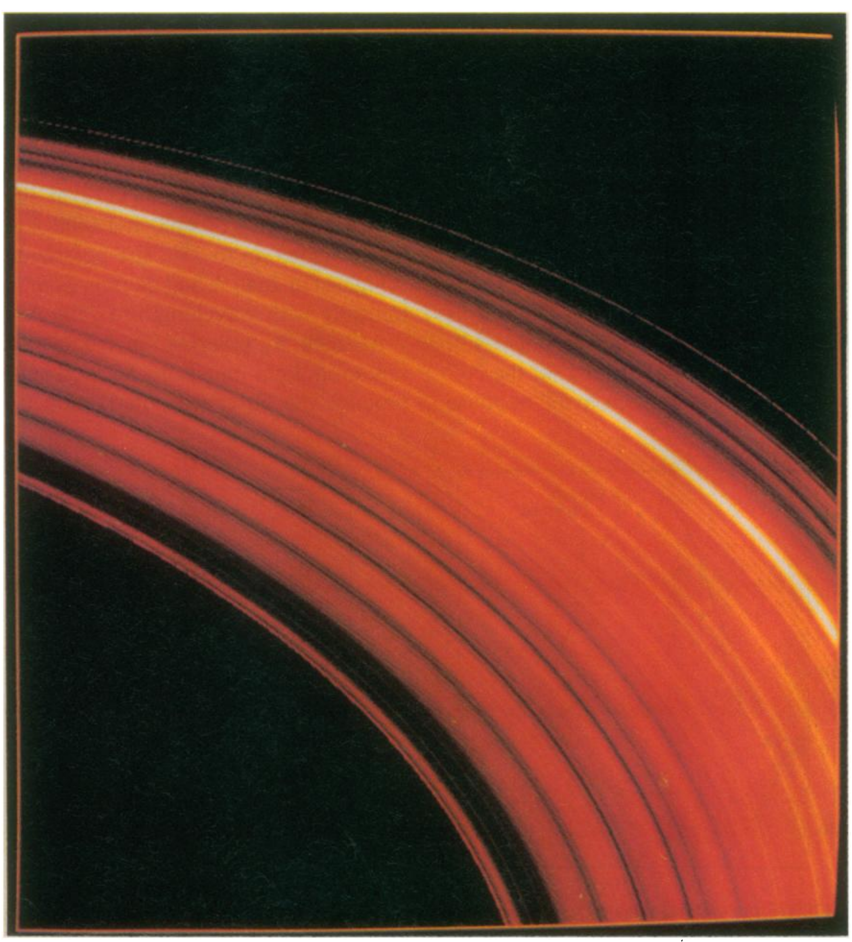

Fig. 7. Computer-generated image of Saturn's F ring made from information obtained from the PPS star occultation. The resolution is approximately 1 km. This portion of the F ring is made of at least ten strands.

scattering and polarization behavior, we will be able to derive its scattering properties from the data without reference to spheres. The next step would be to search for particles with the derived scattering properties. In view of the likelihood that Titan's aerosols are nonspherical (solids), that next step may prove to be quite difficult.

Saturn's rings. On 25 August 1981, the PPS observed the bright ultraviolet star δ Scorpii as it was occulted by Saturn's rings (*21*). The star was observed continuously in the 2640-Å filter of the instrument from its emersion from behind Saturn's disk through the D, C, B, A, and F rings. Every 10 msec the instrument recorded the star brightness and thus the ring opacity: successive data points are separated by a distance of approximately 100 m from Saturn's center. This observation thus provides a continuous cut through the entire ring system with resolution unachievable by other means.

For ease of presentation, we have converted subsets of our data into two-dimensional images, assuming azimuthal symmetry in the rings. These images represent false-color pictures of what an observer or camera might see from a close-up vantage point where the resolution is the same as that provided by the PPS star occultation. Figure 7 shows a view of the main strand of Saturn's F ring, first discovered by Pioneer 11 (*22*). We have degraded our resolution by smoothing over 1-km intervals. The total width of the strand is approximately 40 km and thus would appear as a single feature to the television cameras. We see at least ten individual elements in this strand, but, lacking azimuthal information, we cannot conclude anything about possible braiding.

Figure 8a shows the derived optical depth in the region from which the picture in Fig. 7 was created. The optical depth in the thickest part of the F ring is as large as that in many parts of the A and B rings. How this material is constrained into a region less than 3 km wide is of considerable interest. To examine this, we look at the individual, thickest feature in the F ring at our best resolution (~ 100 m) (Fig. 8b). At that resolution, even this strand shows structure: lower opacity is seen at the center, with ridges at both the inner and outer edge. It appears that material attempting to diffuse out of this feature meets some barrier at the edges. A similar morphology was seen for many broader ringlets by the radio science occultation experiment on Voyager 1 and in the η ring of Uranus (*23*).

Figure 9 shows a two-dimensional representation of the Encke division, a narrow feature in the outer A ring. The resolution is degraded to about 1 km. A regular, wavelike undulation is present in the A ring inward of the gap. The inner edge of the A ring shows both a narrow gap and a narrow ringlet. A multiple ringlet appears in the center of the gap. The imaging team (*24*) has seen a single,

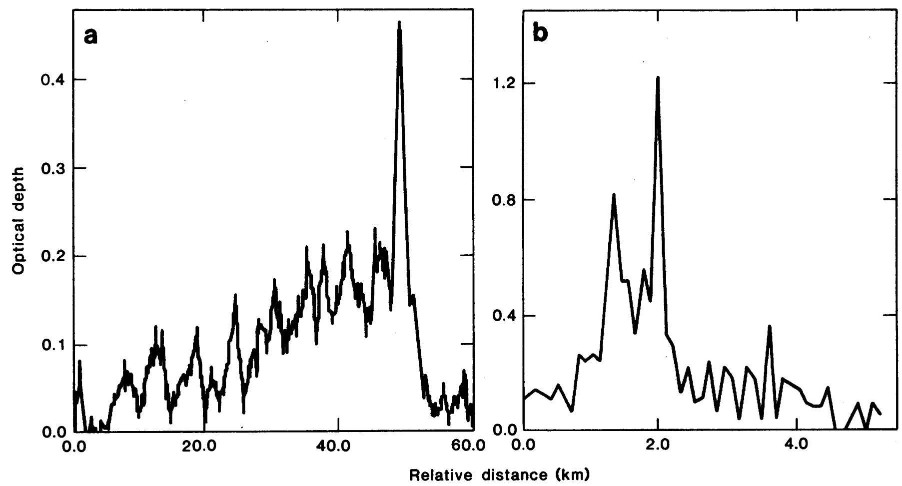

Fig. 8. (a) Optical depth in the thickest part of the F ring. Figure 7 was created from these data. (b) This strand (the optically thickest in the F ring) shows a structure in which particles are concentrated at the edges of the ringlet.

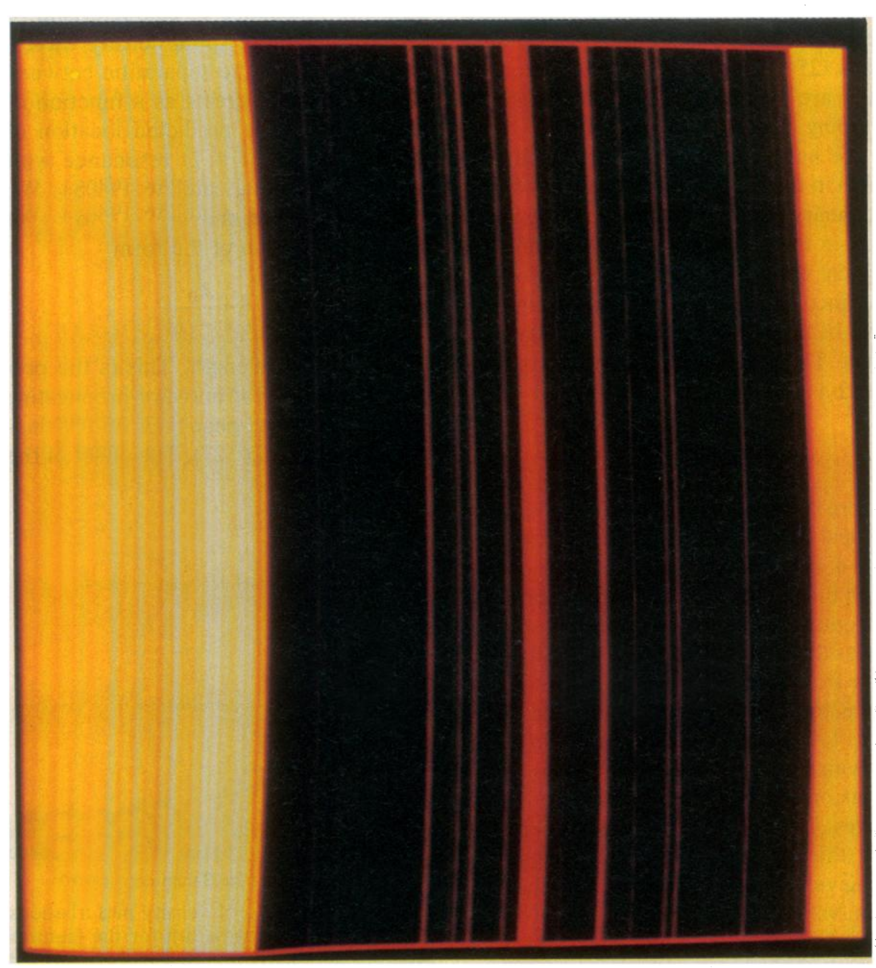

Fig. 9. Encke's division, a narrow gap in the outer A ring, as seen by the PPS star occultation. Waves are evident. The gap contains a multiple ringlet. The resolution is approximately 1 km.

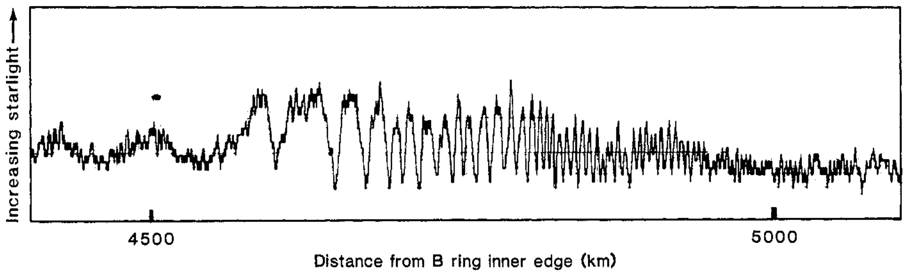

Fig. 10. The raw data in the region of the wave train in the inner B ring.

discontinuous, kinky ringlet at several locations within the Encke gap.

Because our line of sight to the star is not perpendicular to the ring plane, the ray from the star at any instant samples material at different radii from Saturn, unless the ring system is infinitesimally thin. This geometry provides a source of smearing in our data; the smearing length is proportional to the thickness of the ring material in the vertical (perpendicular to the ring plane) direction. By looking at sharp transitions between opaque and transparent regions in the rings, we can find an upper limit to the smearing, which in turn provides an upper limit on the vertical extent of the rings at those locations. These local measurements are preferable to Earth-based determinations (*25*) of the ring thickness because they are not confused by the possible warping of the ring plane itself.

We have examined several such features in the rings. At an absolutely sharp boundary with a rectangular cross section in the radial direction, the inferred optical depth is a linear function of the distance of the observed point from Saturn because of the nonnormal line of sight. The slope of this change in optical depth is

$$\frac{d\tau}{dx} = -\frac{\Delta\tau}{h \tan \theta'} \qquad (1)$$

where $\Delta\tau$ is the magnitude of the jump in optical depth, h is the vertical thickness, and θ' is the angle the line of sight makes with the normal to the ring plane projected onto the radial direction. In several cases the observed slope is indistinguishable from the time response of the instrument to a sudden change in light level. This lower limit to the observable slope sets an upper limit to the thickness of the rings of 200 m at the locations of these edges. Like all earlier measurements of the thickness of the visible rings, we achieve only an upper limit; nonetheless, this value is the smallest ever determined.

The star occultation provides a solid confirmation of the existence of spiral density waves in Saturn's rings. Such waves were first proposed by Goldreich and Tremaine (*26*) to explain the width of the Cassini division. Cuzzi *et al.* (*27*) interpreted features within the Cassini division as a train of such spiral waves of exceptional long wavelength excited by the apsidal resonance of the ring particles with the mean motion of Iapetus. However, the camera resolution limit of 10 km prevented them from seeing waves with shorter wavelengths. One such wave train is seen in our data on the inner B ring.

Figure 10 shows the occultation data in this region. The shortening of the wavelength with increasing distance from the resonance is characteristic of the propagation of spiral density waves. Figure 11 shows the separation between successive wave crests as a function of distance from the predicted location of the 2:1 ($m = 2$, $\ell = 2$) resonance with Saturn's co-orbital satellite 1980S1. We have overplotted the best fit to these data by a function of the form

$$\lambda = \frac{A_0}{x - x_0}$$

where λ is wavelength. This is the predicted behavior for outward-propagating long spiral waves near their inner Lindblad resonance (*26, 27*). The offset of the start of the wave train from its predicted location is given by x_0. We find $x_0 \sim 100$ km; this is consistent with its being at the predicted location within the precision allowed by the preliminary trajectory tape from which the location of the waves was calculated. The parameter A_0 is proportional to the surface mass density of the resonance. Our value gives the mass density $\sigma = 60$ g/cm^2. Cuzzi *et al.* (*27*) have measured σ in the outer Cassini division by the same method. Their value is 16 g/cm^2: this is in good agreement with our result since the average optical depth ($\tau \cong 0.16$) is smaller by a factor of 4 in the Cassini division than in the part of the inner B ring from which the waves are propagating ($\tau \cong 0.6$). Thus, the ratio of optical depth to mass density is the same at the two locations.

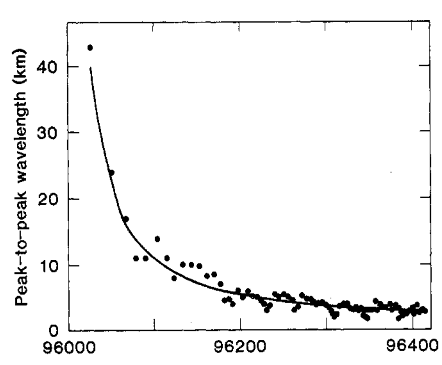

Fig. 11. Wavelength of density perturbations versus distance from Saturn for the features seen in Fig. 10. Overplotted is the expected behavior of an outward-propagating spiral density wave.

Because of conservation of angular momentum and the $1/x$ decrease in wavelength, we expect the wave amplitude to grow linearly with distance from the resonance. Unfortunately, for a resonance as strong as that seen here, the wave must quickly become nonlinear as the predicted fractional amplitude exceeds unity—in fact, in about one wavelength. Our data yield a distance to nonlinearity of less than about 50 km. The calculated distance from the linear theory and an estimate of the mass of 1980S1 [derived by assuming it to be an oblate spheroid with axes given by Smith *et al.* (*24*) and a mass density of 1.2 g/cm^2] gives a theoretical value of 40 km. The two co-orbital satellites are not at exactly the same distance from Saturn, and so their respective wave trains should be offset by about 30 km. We see some slight evidence of beating in the nonrandom residuals in Fig. 11; nonetheless, ~ 80 percent of the mass is in the leading co-orbital (1980S1), and in the above analysis we have considered it alone. This agreement, coupled with the agreement in location in the wavelength dependence and in the local mass density, convinces us that we are actually seeing the propagation of spiral density waves excited by the resonance with the co-orbital satellites.

Goldreich and Tremaine (*26, 28*) provided a formulation to calculate viscous losses due to interparticle collisions. From our data, the decrease in amplitude gives a damping length of ~ 300 km. If this is due entirely to viscous effects, it implies a kinematic viscosity, $\upsilon \cong 20$ cm^2/sec. From Goldreich and Tremaine (*26*), we have

$$\upsilon = \frac{c^2}{2\Omega}\left(\frac{\tau}{1+\tau^2}\right)$$

where c is the one-dimensional velocity dispersion and Ω is the angular orbital velocity. Solving for c gives $c \sim 0.1$ cm/sec, an average random velocity of 1 mm/sec.

There are several reasons why we should treat this value with caution. First, this analysis assumes equal-sized particles: in a medium with particles of many sizes, equipartition of energy leads to different velocities for each particle size. Second, this formulation neglects interparticle gravitational interactions (*29*). This small velocity is less than the free-fall velocity onto a 10-m particle, and so gravitational focusing and scattering could be just as important. Third, if we calculate Toomre's stability criterion (*30*),

$$Q \equiv \frac{Kc}{\pi G \sigma}$$

where K is the epicyclic frequency of a particle and G is the gravitational constant, then $Q \sim 2$. This means that the disk is only marginally stable to axisymmetric collapse (*30*). This also violates an assumption of Goldreich and Tremaine (*28*). In summary, the physical situation gives little confidence in the calculation of the random velocity: at best, a value for c of ~ 0.1 cm/sec gives only an upper limit; more likely, only the largest particles in a steep particle size distribution actually obey this upper limit. The vertical excursion of monodisperse particles in the ring with random velocity c (for $c \sim 1$ mm/sec) is

$$h \sim \frac{c}{\Omega} = 10 \text{ m}$$

This provides a theoretical vertical thickness for the rings which is comfortably inside our observed upper limit of 200 m (see Eq. 1).

What are the implications of these findings for the structure and evolution of Saturn's rings? The basic question remains: What causes and maintains the multitude of structures visible in Saturn's rings? A popular view before the Voyager 2 flyby was that most of these structures were due to embedded moonlets (*31*). However, an exhaustive search was made by the imaging team for the largest of these, and none was found (*24*). Even moonlets too small to be seen by the cameras would leave small gaps in the rings with a width of $\geqslant 2$ km; these could easily be resolved by the PPS occultation. An in-depth look at several regions of our data shows no evidence of such gaps.

Goldreich and Tremaine (*26*) suggested that angular momentum carried by spiral density waves could clear broad gaps such as the Cassini division. The confirmation of the existence of such waves from the Voyager data supports such a mechanism. Nonetheless, our data are not consistent with this idea as a complete explanation. For example, we see no gap whatever at one location (see Fig. 10). A simple application of the spiral wave–clearing mechanism would predict a gap of width 40 km to be opened in less than 10^5 years.

Our data are consistent with a mechanism of dynamic instability proposed by Ward (*32*) and Lin and Bodenheimer (*33*). In this model, an instability grows in which the low-density regions of the rings depopulate themselves by viscous interactions with the neighboring material. The velocity dispersion decreases in the thicker regions while it increases in the thinner regions. A comparison of our derived dispersion velocity in the inner B ring ($c \leqslant 0.1$ cm/sec; $\tau = 0.6$) with that found by Cuzzi *et al.* (*27*) ($c \leqslant 0.6$ cm/sec; $\tau = 0.14$) does not contradict this model. However, since other mechanisms may contribute to wave damping, these values for c are upper limits; thus, we cannot construe this argument as support for this instability.

These findings suggest that the ring structure is much more dynamic than was earlier believed. The influence of permanent structures created by moons is surely insufficient. Features such as density waves, gravitational instabilities, and dissipative instability may play the dominant role. As the above determinations of ring mass density and viscosity show, we now have an opportunity to probe the physical nature of the ring system through its dynamic interactions.

ARTHUR L. LANE
Jet Propulsion Laboratory,
California Institute of Technology,
Pasadena 91109

CHARLES W. HORD
ROBERT A. WEST
LARRY W. ESPOSITO
Laboratory for Atmospheric and
Space Physics, University of
Colorado, Boulder 80309

DAVID L. COFFEEN
MAKIKO SATO
Goddard Institute for Space
Studies, New York 10025

KAREN E. SIMMONS
Laboratory for Atmospheric and Space
Physics, University of Colorado

RICHARD B. POMPHREY
RICHARD B. MORRIS
Jet Propulsion Laboratory,
California Institute of Technology

References and Notes

1. C. W. Hord, R. A. West, K. E. Simmons, D. L. Coffeen, M. Sato, A. L. Lane, J. T. Bergstralh, *Science* **206**, 956 (1979); R. A. West, *Geophys. Res. Lett.* **8**, 847 (1981).
2. R. A. West, C. W. Hord, K. E. Simmons, D. L. Coffeen, M. Sato, A. L. Lane, "Near ultraviolet scattering properties of Jupiter," *J. Geophys. Res.* **86**, 8783 (1981).
3. C. F. Lillie, C. W. Hord, K. Pang, D. L. Coffeen, J. E. Hansen, *Space Sci. Rev.* **21**, 159 (1977).
4. E. C. Stone and E. D. Miner, *Science* **215**, 499 (1982).
5. The results will be reported later (A. L. Lane, C. W. Hord, R. A. West, L. W. Esposito, D. L. Coffeen, M. Sato, K. E. Simmons, R. B. Pomphrey, R. B. Morris, in preparation).
6. B. A. Smith *et al.*, *Science* **212**, 163 (1981).
7. R. Hanel *et al.*, *ibid.* **204**, 972 (1979); R. Hanel *et al.*, *ibid.* **206**, 952 (1979); A. L. Broadfoot *et al.*, *ibid.* **204**, 979 (1979).
8. A. L. Broadfoot *et al.*, *ibid.* **212**, 206 (1981).
9. N. F. Ness, N. H. Acuna, R. P. Lepping, K. W. Behannon, L. F. Burlaga, F. M. Neubauer, *Nature (London)* **280**, 799 (1979).
10. The spatially resolved data will be reported later (A. L. Lane, C. W. Hord, R. A. West, L. W. Esposito, D. L. Coffeen, M. Sato, K. E. Simmons, R. B. Pomphrey, R. B. Morris, in preparation).
11. Of the eight positions on the analyzer wheel, only four are available because of a command logic failure which occurred at Jupiter flyby. Two of the four remaining positions are redundant.
12. M. G. Tomasko, *J. Geophys. Res.* **85**, 5937 (1980).
13. J. Veverka, *Icarus* **18**, 657 (1973): B. Zellner, *ibid.*, p. 661; M. Podolak and R. E. Danielson, *ibid.* **30**, 479 (1977).
14. M. Podolak and L. P. Giver, *ibid.* **37**, 361 (1979).
15. K. Rages and J. B. Pollack, *ibid.* **41**, 119 (1980).
16. K. Rages, personal communication.
17. J. E. Hansen, *J. Atmos. Sci.* **28**, 1400 (1971). We use the "standard" size distribution $n(r)$ = constant $r^{(1-3b)/b}\, e^{-r/ab}$, where $\bar{r} = a$ and b is the effective variance.
18. ———, *Astrophys. J.* **155**, 565 (1969).
19. H. G Horak, *ibid.* **112**, 445 (1950).
20. O. B. Toon, R. P. Turco, J. B. Pollack, *Icarus* **43**, 260 (1980); M. G. Tomasko, personal communication.
21. The idea of using the Voyager photopolarimeter instrument to perform a stellar occultation of Saturn's rings was originally proposed in 1972 by C. F. Lillie, then at the Laboratory for Atmospheric and Space Physics, University of Colorado.
22. T. Gehrels *et al.*, *Science* **207**, 434 (1980).
23. G. L. Tyler, public communication at the Voyager 2 press conference, 1981; J. L. Elliot, R. G. French, J. A. Frogel, J. H. Elias, D. J. Mink, W. Liller, *Astron. J.* **86**, 444 (1981).
24. B. A. Smith *et al.*, *Science* **215**, 504 (1982).
25. K. Lumme and W. M. Irvine, *Astron. Astrophys.* **71**, 123 (1979).
26. P. Goldreich and S. Tremaine, *Icarus* **34**, 240 (1978).
27. J. N. Cuzzi, J. J. Lissauer, F. H. Shu, *Nature (London)* **292**, 703 (1981).
28. P. Goldreich and S. Tremaine, *Icarus* **34**, 227 (1978).
29. J. N. Cuzzi, R. H. Durisen, J. A. Burns, P. Hamill, *ibid.* **38**, 54 (1979).
30. A. Toomre, *Astron. J.* **139**, 1217 (1964).
31. J. J. Lissauer, F. H. Shu, J. N. Cuzzi, *Nature (London)* **292**, 707 (1981).
32. W. R. Ward, *Geophys. Res. Lett.* **8**, 641 (1981).
33. D. N. C. Lin and P. Bodenheimer, *Astrophys. J. (Lett.)* **248**, L83 (1981).
34. The PPS team thanks the Voyager Project and especially the numerous members of the Voyager Flight Team who worked beyond our expectations to help the photopolarimeter have such a successful encounter. We thank G. McNutt for his tireless engineering support. We also acknowledge with our appreciation J. N. Cuzzi, J. B. Pollack, K. Rages, S. D. Tremaine, J. L. Elliot, and M. G. Tomasko for helpful discussions; R. E. Steele and M. E. Ockert for computing assistance; and J. J. Lissauer and J. N. Cuzzi for tabulated information on resonances in Saturn's rings. We thank M. G. Tomasko for kindly supplying a polarization doubling code.

12 November 1981